



# Influence of Penetration Angles on Global-Thermo-Hydraulic-Performance of Shell and Tube Heat Exchangers with Multi-Cross Sectional Tube Configurations

<sup>1\*</sup>Alabi I. O., <sup>2</sup>Ademola A. D, and <sup>2,3</sup>Petinrin M. O.

<sup>1</sup>Department of Mechanical Engineering, Elizade University Ilara-Mokin, Ondo State, Nigeria.

<sup>2</sup>Department of Mechanical Engineering, University of Ibadan, Nigeria.

<sup>3</sup>School of Mechanical Engineering, Fiji National University, Suva, Fiji.

<sup>1</sup>[ismaila.alabi@elizadeuniversity.edu.ng](mailto:ismaila.alabi@elizadeuniversity.edu.ng) <sup>2</sup>[ademola\\_dare@yahoo.com](mailto:ademola_dare@yahoo.com) <sup>3</sup>[layopet01@yahoo.com](mailto:layopet01@yahoo.com)

## Article Info

### Article history:

Received: Dec. 17, 2024

Revised: Jan. 22, 2025

Accepted: Jan. 25, 2025

### Keywords:

Shell-and-tube heat exchanger, Tube-Geometry, Penetration angles, Thermo-hydraulic performance indices.

### Corresponding Author:

[ismaila.alabi@elizadeuniversity.edu.ng](mailto:ismaila.alabi@elizadeuniversity.edu.ng)

+2348060849804

## ABSTRACT

*Shell-and-Tube Heat Exchanger (STHE), a vital component for efficient energy management when used with Straight-Tube Geometries (STG) is associated with low Global-Thermo-Hydraulic-Performance (GTHP). These contribute to the high energy demand of processing plants. The recently developed STHEs with modified tube configurations have not adequately addressed these limitations and necessitated a continuous search for improved-performance tubes. Multi-cross-sectional tube geometrical (MSTG) configurations improve GTHP along flow lines. This process has not been thoroughly investigated. Therefore, this study was designed to examine the influence of penetration angles (PAs) on the STHEs' performances using MSTG configurations. The numerical analysis was evaluated in terms of GTHP indices on STHE with Convergent-Divergent-Tube-Geometry (CDTG) and Divergent-Convergent-Tube-Geometry (DCTG) configurations of varying penetration angles (PAs), 0,5,10,15,...,90°. Numerical GTHP for STHE with STG was 1.0, while that obtained for STHE with CDTG configurations for all PAs fell between 1.50 to 1.625 with the highest at 5° PA indicating a 50% minimum improvement in GTHP over STHE-STG. For DCTG, GTHP were between 1.43 and 1.585 for all PAs with the highest at 5° PA indicating a 43% minimum improvement in GTHP over STHE-STG. Replacing STHE-STG with STHE-MSTG can improve their GTHPs in processing plants.*

## INTRODUCTION

Shell-and-Tube Heat Exchangers (STHEs) are a class of tubular heat exchangers used in various industrial processes and areas (Mohammad *et al.*, 2020). Their superior advantages and applications have contributed to their simple manufacture and suitability under various working conditions. They can move two fluids in two distinct phases and opposite directions (Shirvan *et al.*, 2018). The main component of the STHE system is a group of tubes positioned with their axis parallel to the shell inside a sizable cylindrical shell. The purpose of the system is to move heat across two distinct fluids, which may be gasses or liquids on the tube or shell side, either

through the tube walls from the tube side to the shell side, or the other way around, thereby balancing the temperature. In STHE, there are numerous distinct procedures and events (Olaiya *et al.*, 2018).

As a function of Pressure Drop (PD), the efficiency of STHEs in thermal energy transfer at low pumping power results in a significant decrease in energy consumption, which raises the plants' financial gain. Therefore, in plants with a network of STHEs, the functions of these interconnected HEXs become increasingly important for meeting the plants' energy needs. This is because the thermo-hydraulic efficiency of STHEs is crucial to the overall

performance of the plants in many industrial processes.

Literature rarely describes the tube-side cross-sectional structure of the STHEs. Saffarian *et al.* (2019) provided a combined STHE model with elliptical and circular tubes at a 90° attack angle. When compared to STHEs with circular tubes and elliptical tubes at attack angles of 90° and 0°, the heat exchanger with ellipsoidal tubes near the shell and circular tubes at the center of the shell exhibited the highest heat transfer. For every of the experiment's five scenarios, the pressure drop in the tube and shell side was examined as well.

Slimene *et al.* (2021) numerically modeled a rectangular shell-and-tube heat exchanger and discovered that the overall high effectiveness of their design was due to the rectangular cross-section shell, which outperforms its cylindrical equivalent when compared to data from the literature. Wang *et al.* (2018) conducted an experimental and numerical investigation into the heat transfer and flow characteristics on the shell side of a Helically Coiled Trilobal Tube (HCTT) heat exchanger. The Helically Coiled Elliptical Tube (HCET) and Helically Coiled Plain Tube (HCPT) showed lower field synergy numbers than the HCTT, indicating that the HCTT effectively improved flow and heat transmission.

Nonetheless, research has also been done on corrugated tubes as a coarsening surface technique. Gondane and Jibhakate (2018) found that the STHE with a corrugated tube had the highest convective heat transfer coefficient value. Three different tube bundles were examined by Prabakaran *et al.* (2016) for a particular heat exchanger: smooth, micro-finned, and corrugated tubes with pressure drop and heat transfer rate. It was discovered that corrugated tubes outperformed other materials in terms of performance.

Most of the previous research reviewed has been on STHEs' Straight-Tube Geometries (STG), which are associated with low heat duty and significant pressure drops, both of which raise a plant's energy requirements. However, recent altered tube designs of STHEs have not been able to adequately address these limitations, which have led to current work focusing on tubes with improved performance.

A perfect scenario for pipe flow obstructions is for the flow to increase in pressure while decreasing in velocity, which signifies that the fluid flow pressure and flow velocity are inversely correlated. However, it is expected that under this scenario the pressure drop should be drastically reduced. Anytime there is sudden enlargement or contraction in flow due to the addition of divergent or convergent pipes, the flow velocity is significantly reduced at the point of convergence-divergence while the fluid flow pressure rises, leading to a low-pressure drop. Multi-cross-sectional tube geometrical (MSTG) layouts improve fluid pressure along flow lines. This mechanism has not been completely researched. Using an STHE with both Divergent-Convergent Tube Geometrical (DCTG) and Convergent-Divergent Tube Geometrical (CDTG) configurations, Alabi *et al.* (2024) examined the impact of MSTG configurations on the performances of the STHEs. It was determined that better performance resulted from shell and tube heat exchanger designs that included MSTG. The study's shortcoming is that it only examined configurations with penetration angles (PAs) of 45 and 90 degrees, which was insufficient to predict an STHE with the best possible global thermohydraulic performance (GTHP). As a result, the purpose of this study was to examine how various penetration angles (PAs) and MSTG configurations, such as divergent-convergent and convergent-divergent tube configurations, affected the performance of the STHEs

**METHODOLOGY**

In this investigation, STHE with three distinct tube configurations; divergent-convergent tube geometries (DCTG), convergent-divergent tube geometries (CDTG), and straight tube geometries (STG) created from CREO-Parametric CAD software were numerically simulated using finite volume-based ANSYS FLUENT 19.2 software. The simulation was conducted on a computer system equipped with an Intel® Core™ i7 2.50 GHz CPU and 16 GB of RAM. In every heat exchanger analysis, the working fluid flow arrangements at the shell and tube inlets were counter-flow directions. The impact of the tube's construction on heat exchanger efficacy was also assessed by taking into account the fluid pressure drop on the tube side.

*Geometry Parameters and Configurations of Selected STHEs*

The convergent-divergent (CD) and divergent-convergent (DC) with 5 to 90° penetration angles, 30° triangular tube architecture, and 25% horizontal cut single-segmental baffles were among the innovative tube designs as shown in Figure A of Appendix A that were investigated because of their strong heat transmission properties. Single-segmental baffled straight-tube geometrical configurations have been commonly used as benchmarks for comparison due to their prominence in the STHE industries (Mukherjee, 1998). It also provided the basis for comparison in this investigation. The geometrical characteristics of the selected STHEs used in this investigation are shown in Table 1:

Using the relationship in equations 1 and 2 derived from Sinnott (2005), the shell interior diameter was calculated from Table 1 based on the tube bundle diameter,  $D_b$ .

$$D_b = d_o \left( \frac{N_t}{K_o} \right)^{n_o} \tag{1}$$

$$D_s = D_b + C_{sb} \tag{2}$$

where  $d_o$  is the outside diameter of the tube,  $n_o$  and  $K_o$  are constants, and  $N_t$  is the number of tubes with an example, with a one-tube pass STHE and a triangle pitch of  $1.25d_o$ ,  $K = 0.319$  and  $n = 2.142$ .

Table 1. Geometry Parameters of Selected STHE

Component	Description	Value
<b>Baffle</b>	Number of baffles	1-4
	Baffle spacing	90 - 225 mm
	Diameter of the baffle plate	105 mm
	Baffle hole (diameter), Baffle cut	15 mm, 25%
<b>Tube-side</b>	Tube diameter (divergent part), $d_{dt}$	$\phi$ 15 mm
	Tube diameter (convergent part), $d_{ct}$	$\phi$ 10 mm
	Inlet & outlet diameter (control)	$\phi$ 15, 13 mm
	Tube length (Total), $L_T$	450 mm
	Layout pattern	Triangular (30°)
<b>Shell-side</b>	Pitch	$1.25d_{dt}$
	Shell inside diameter, $D_s$	105 mm
	Shell outside diameter, $D_E$	107 mm
	Length of shell	450 mm

Moreover,  $C_{sb}$  stands for shell-bundle clearance, and the shell-bundle clearance chart was used to

determine the value of  $C_{sb}$  for the outer packed head STHE.

*The Thermo-physical Properties of Fluids and Shell-and-Tube Heat Exchanger Materials*

In this study, water is the only working fluid considered from both the shell and tube sides. The fluid materials employed in this work and the shell and tube's thermo-physical properties are as presented in Alabi et al., (2024).

*Computational modeling*

The conservation of mass, momentum, and energy provided a basis for the fluid flow models and heat transfer in the selected STHEs. Turbulence terms are incorporated into the equations due to the significant amount of turbulent fluid flow.

Assumptions

The models were created with the following assumptions in mind:

- a. The flow was assumed incompressible and turbulent.
- b. Fluid was assumed single-phase Newtonian.
- c. The fluid's physical properties are constant.
- d. There was no thermal radiation, no gravity effect, no volume force nor heat source.
- e. The Leakages between the baffle and the tubes were assumed to be negligible.

The STHE had been predicted to have tiny shell-side fouling resistance, even though this was not considered in the energy formulation.

Governing Equations

A hydrodynamic model based on the unstructured-grid finite volume approach was constructed using ANSYS. The continuity, momentum, and energy solution served as the foundation for the model (Naqvi and Wang, 2019):

#### A. Continuity equation:

The continuity equation is s given in equation (3)

$$\rho \nabla \cdot \mathbf{u} = 0 \quad (3)$$

#### B. Momentum equation:

The momentum equation is s given in equation (4)

$$\rho \mathbf{u} \cdot \nabla \mathbf{u} = -\nabla P + \nabla \cdot (\mu + \mu_T) [\nabla \mathbf{u} + (\nabla \mathbf{u})^T] - \frac{2}{3} \rho k I \quad (4)$$

#### C. Energy equation:

The energy equation is s given in equation (5)

$$\nabla (\rho c_p \mathbf{u} T - k \cdot \nabla T) = 0 \quad (5)$$

#### D. Turbulent model:

Turbulence on the shell side of STHEs easily starts due to the tortuous flow pattern formed by the baffles and tube bundles (Kuppan, 2013). Therefore, in addition to these equations, the Two-Equation Reynolds-Averaged Navier-Stokes (RANS) turbulent (k-ε) model was selected because it predicts well far away from the boundaries (wall) and is provided below (Alfarawi, 2020):

- i. Turbulent kinetic energy equation (k):  $\rho \frac{\partial k}{\partial t} + \rho \mathbf{u} \cdot \nabla k = \nabla \cdot \left( \left[ \mu + \frac{\mu_T}{\sigma_k} \right] \nabla k \right) + P_k - \rho \varepsilon \quad (6)$

$$P_k = \text{Production term} = \mu_T [\nabla \mathbf{u} : (\nabla \mathbf{u} + (\nabla \mathbf{u})^T)] \quad (7)$$

Where,  $\nabla \cdot \left( \left[ \mu + \frac{\mu_T}{\sigma_k} \right] \nabla k \right)$  is the diffusion term;

- ii. Turbulent energy dissipation rate equation (ε):

$$\rho \frac{\partial \varepsilon}{\partial t} + \rho \mathbf{u} \cdot \nabla \varepsilon = \nabla \cdot \left( \left[ \mu + \frac{\mu_T}{\sigma_\varepsilon} \right] \nabla \varepsilon \right) + C_{\varepsilon 1} \frac{\varepsilon}{k} P_k - C_{\varepsilon 2} \rho \frac{\varepsilon^2}{k} \quad (8)$$

$$\mu_T = \text{Turbulent viscosity} = \rho C_\mu \frac{k^2}{\varepsilon} \quad (9)$$

The model closure constants are:  $C_{\epsilon 1} = 1.44$ ;  $C_{\epsilon 2} = 1.92$ ;  $C_{\mu} = 0.09$ ;  $\sigma_k = 1.0$ ;  $\sigma_{\epsilon} = 1$ . (Saffarian *et al.* 2019)

**Boundary Conditions, Solvers Selection, and Mesh Description**

The solutions to the governing equations are significantly influenced by the physical state of the boundaries of the computational domain (Bergman, 2011). The mass flow, temperature, and pressure boundary conditions that are applied to the tube side and shell sides, respectively, are displayed in Table 2. The selected values were consistent with the research work of Petinrin (2016). The gauge pressure was used as the outlet pressure for applying the Dirichlet boundary conditions at the outlets of the tubes and shell. Because of the separated technique's memory efficiency, adaptability, and resilience in handling nonlinear multi-physics problems including conjugate heat transfer, multiphase, and combustion problems (Kelecy, 2008), a segregated method was chosen as the method for solving the computational problems in this work. In each of the selected designs, the fine mesh was created around the shell, tube, and baffles to increase accuracy and result in quality. The range of grids generated from the series of independence tests that were done falls between 1343231 and 2138820 elements, from the meshing nodes between 369549 and 612956, based on the correctness of the results in a short amount of time. Depending on the complexity of the buildings and other input criteria, each simulation required a minimum of nine hours. A mesh that was made for one of the models is shown in Figure 1.

**Performance criteria**

When assessing and studying the thermo-hydraulic performance of any heat exchanger, two important parameters that need to be considered are heat duty and pumping power.

Table 2. Boundary conditions

Boundary	Boundary type	values
Inlet shell	Mass flow inlet	0.6 - 2.1 kg/s & 300.15 K
Outlet shell	Pressure outlet	0 Pa (Gauge pressure)
Inlet tube	Mass flow inlet	0.05 kg/s & 373.15 K
Outlet tube	Pressure outlet	0 Pa (Gauge pressure)
Shell wall	Wall, stationary, no-slip, adiabatic	adiabatic

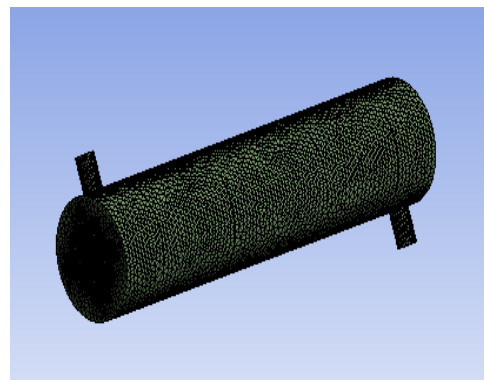


Figure 1. Mesh Generation

The heat duty is a function of the heat transfer coefficient, also known as the Nusselt number, whereas the pumping power is a function of the pressure drop (or drag coefficient and friction coefficient for shell and tube, respectively) (Kuppan, 2013). To assess the performance of the recently developed shell and tube heat exchangers, a numerical analysis was done. Here, the findings were examined using seven Global Thermo-Hydraulic Performance (GTHP) standards. These include the Performance Evaluation Index (PEI), Performance Evaluation Criterion (PEC), Shell Gain Performance Factor (SGPF), Thermal Performance Factor (TPF), Weighted Shell Heat Transfer Coefficient (WSHTC), Field Synergy Number (FSN) and Effectiveness ( $\epsilon$ ), (see Appendix B).

**RESULTS AND DISCUSSION**

*Mean flow and thermal fields*

The velocity maps, as well as the impact of the various penetration angles (PAs) and MSTG configurations on heat transfer and flow characteristics in a shell and tube heat exchanger at the same operating conditions, are among the results of mean flow and thermal fields presented in this subsection.

Velocity Profile

The velocity profile of the selected STHEs from 5 to 90 degrees Penetration Angle (PA) with 0 repeats in comparison with the baseline is presented in Figure A of Appendix C. The velocity profiles make it easier to discern that flow velocity increases in the area between the bottom of the shell and the edge of the first baffle. In addition, there was no difference in flow patterns between STHE-CDTGs and STHE-DCTGs with a 10 – 45-degree penetration angle under the same mass flow rate. But about every heat exchanger, the fluid velocity is seen to reduce as the fluid enters and moves through the shell side and increases again as it approaches and reaches the shell outlet. This behaviour is expected as the flow area between the shell and all the tubes is much larger than those at the shell inlet and outlet because the law of conservation of mass must be obeyed by the essentially incompressible shell-side fluid flow. It is apparent that boundary layer separation and recirculation zones occur at the rear close to the baffle tip subsequently creating a pattern of zigzag flow required within the shell side of STHEs with segmental baffles (Du and Du, 2019). However, the heat exchangers with 5 degrees penetration angles were found to relatively offer slight deflection thereby causing smooth fluid flow as well as low recirculation along the shell side with fewer dead zones. This enhances proper mixing and better uniform flow in such heat transfer devices. This conclusion is in line with Zahid et al., (2023).

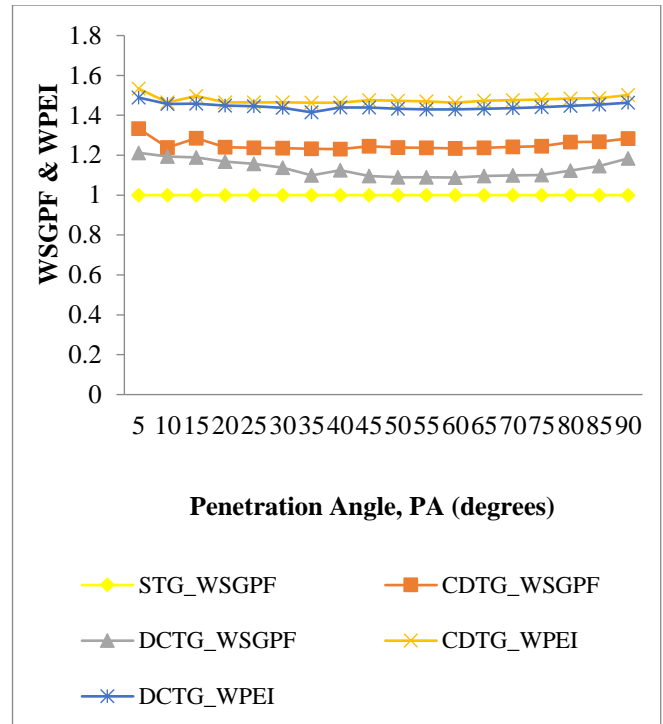


Figure 2. WSGPF and WPEI of the STHE against PA

The Variation of Thermo-hydraulic Performance Factors with angle of penetrations

Results of global thermo-hydraulic performance (GTHP) of STHEs with multi-cross sectional tube geometrical configuration under various penetration angles as compared to the straight tube geometrical configuration are presented in Figures 2 to 4 using the seven global performance parameters. These were obtained under the same mass flow rates. It can be observed that the WSGPF and WPEI values obtained in Figure 2 were higher in STHE-CDTG and STHE-DCTG under various angles of penetration and at the same mass flow rate as compared to baseline (STG). The results ( $1.3 \leq WSGPF \leq 1.50$ ) obtained appreciate well in comparison to that ( $WSGPF \geq 1.0$ ) observed by Petinrin (2016), ( $0.3 \leq WSGPF \leq 0.7$ ) reported by Li et al. (2020) and ( $0.5 \leq WSGPF \leq 1.20$ ) reported by Naqvi and Wang (2019). The results ( $1.3 \leq WPEI \leq 1.43$ ) obtained appreciate by 4.2% in comparison to that ( $1.27 \leq WPEI \leq 1.37$ ) observed by Luo et al. (2021). The best STHE with the highest thermo-

hydraulic performance was obtained at a 5-degree angle of penetration.

It can also be observed that the WPEC and  $\epsilon$  values obtained in Figure 3 were higher in STHE-CDTG and STHE-DCTG under various angles of penetration and at the same mass flow rate as compared to baseline (STG). The values of WPEC obtained in this study (0.63 – 0.67) are a bit lower in comparison to those (1.35 ± 0.1) and (1.5±0.1) (Wang et al. 2018; Slimene et al. 2022), respectively. Additionally, the values of  $\epsilon$  obtained in this study (0.79 – 0.83) are more in comparison to those (0.49 ± 0.3) and (0.2±0.05) reported by Slimene et al. (2022) and Mohammad et al. (2020), respectively. The best STHE with the highest thermo-hydraulic performance was obtained at a 5-degree angle of penetration.

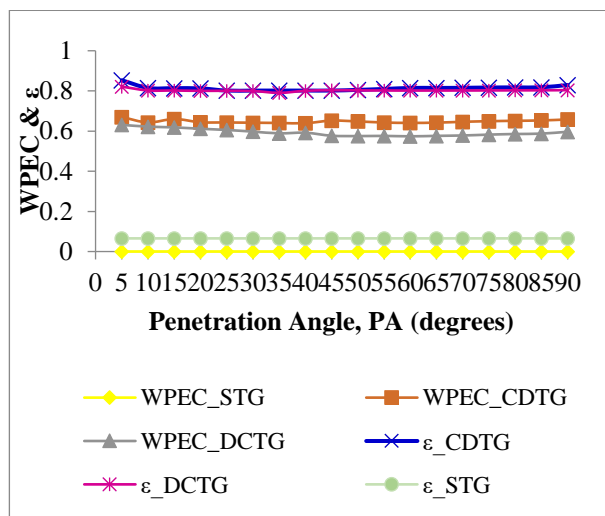


Figure 3. WPEC and  $\epsilon$  of the STHE against PA

It can be observed that the WTPF, WFSN, and WSHTC values obtained in Figure 4 were higher in STHE-CDTG and STHE-DCTG under various angles of penetration and at the same mass flow rate as compared to baseline (STG). The values of WTPF obtained in this study (1.48 – 1.53) are within the range of (1.75 ± 0.4) (Alfarawi, 2020; Shirvan et al. 2018). In addition, the values of WSHTC obtained in this study (1.44 – 1.49) are more in comparison to that (1 – 1.06) reported (Petinrin and

Dare, 2020). The values of WFSN obtained in this study (1.60- 1.61) are more in comparison to that (1.08±1) reported by Wang et al. (2018). The implication of negative values of WFSN (both CDTG and DCTG) between 80 and 90 degrees is that having STHE-MSTG of those angles will not yield any appreciable result in terms of WFSN, it would rather produce exchangers with low thermal performance compared to STHE-STG.

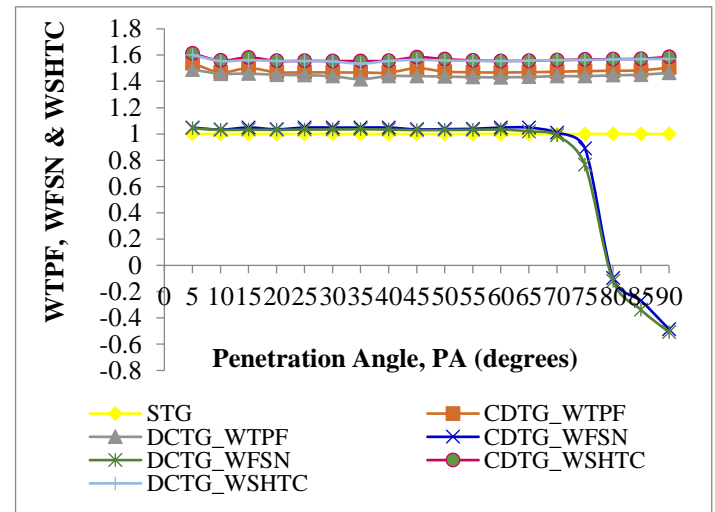


Figure 4. WTPF, WFSN, and WSHTC of the heat exchanger against the angle of penetration

*The Variation of Thermo-hydraulic Performance Factors with mass flow rates at 5 degrees angle of penetrations*

Results of global thermo-hydraulic performance (GTHP) of STHEs with multi-cross-sectional tube geometrical configuration under various mass flow rates as compared to the straight tube geometrical configuration are presented in Figures 5 to 6 using the seven global performance parameters. These were obtained under the same angles of penetration, precisely 5 degrees.

It can be observed that the WSGPF, WPEI, WTPF, WSHTC, and WFSN values obtained in Figure 5 were higher in STHE-CDTG and STHE-DCTG under various Flow Rates (FR) and at the same penetration angles as compared to the baseline

(STG). The WSHTC for the STHE-CDTG and STHE-DCTG at each mass flow rate will be more desirable in terms of thermal performance than the STHE-STG since the values of WSHTC for STHEs with multi-cross-sectional tube configurations are more than one (1) obtained in the baseline (STHE-STG) (Petinrin, 2016). Also, shows that, under the same PA (i.e. 5°), there is a high synergy between the speed and the temperature gradient when STHE-CDTG and STHE-DCTG) at 0.6 kg/s, which leads to a higher heat transfer. This outcome is consistent with the findings of Jiao *et al.* (2022). It can also be observed that the WTPF for the STHE-CDTG and STHE-DCTG at each mass flow rate will be more desirable in terms of thermal performance than the STHE-STG. When compared to the baseline, the MSTGs have an efficient energy exchange rate. The resulting results are consistent with Alfarawi's (2020) observations of  $1.75 \leq WTPF \leq 2.15$ . Additionally, it was found that, as Shirvan *et al.* (2018) also noted, the value of WTPF grows when the shell-side fluid's (cold water) flow rate increases, where the WTPF is larger than unity. Therefore, STHE-MSTGs are superior in terms of energy savings. All the selected STHEs with multi-cross-sectional tube configurations produced higher values of performance factors at 0.6 kg/s. Though, the best result was produced at 1.6 kg/s, not all the selected performance indices gave outstanding performance at 1.6 kg/s.

It can be observed that the WPEC and  $\epsilon$  values obtained in Figure 6 were higher in STHE-CDTG and STHE-DCTG under various mass flow rates and at the same angles of penetration as compared to the baseline (STG). The values of WPEC and  $\epsilon$  obtained for STHE with STG, CDTG, and DCTG were (0.0,  $0.26 \pm 0.1$ ), ( $0.77 \pm 0.1$ ,  $0.87 \pm 0.1$ ) and ( $0.73 \pm 0.1$ ,  $0.83 \pm 0.1$ ), respectively.

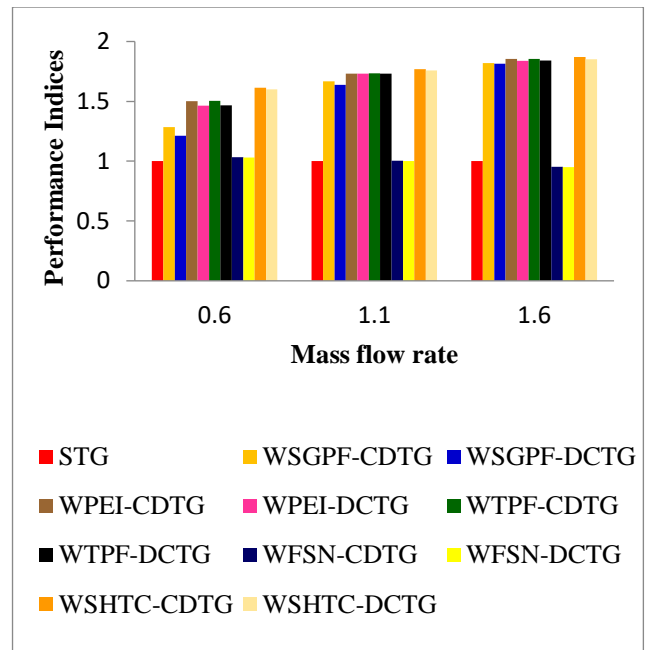


Figure 5. Five-performance indices at a fixed multi-cross-sectional number of repeat and penetration angle

All the selected STHEs with multi-cross-sectional tube configurations produced higher values of performance factors across all ranges of mass flow rates, that is 0.6 – 2.1 kg/s.

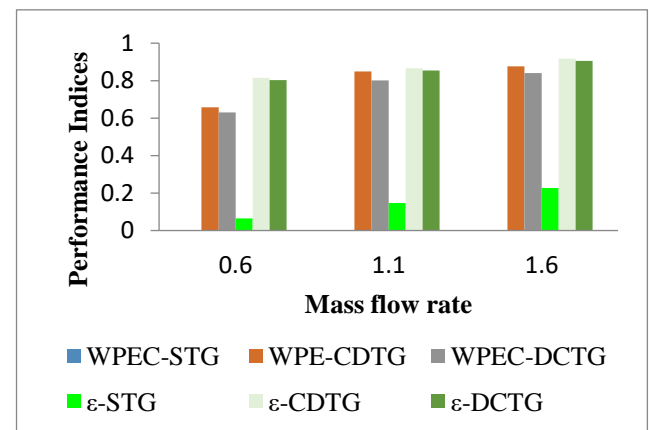


Figure 6. WPEC and  $\epsilon$  fixed multi-cross-sectional number of repeat & penetration angle

It can be observed that the WPEC for the STHE-CDTG and STHE-DCTG at each mass flow rate will be more desirable in terms of thermo-hydraulic performance evaluation than the STHE-STG. The outcome is consistent with the findings of



Mohammad *et al.* (2020), as heat duty outperforms pressure drop. The effectiveness ( $\epsilon$ ) for the STHE-CDTG and STHE-DCTG at each mass flow rate will be more desirable in terms of thermal performance than the STHE-STG. The outcomes were better than the 49–76% that Slimene *et al.* (2021) obtained.

#### CONCLUSIONS AND RECOMMENDATION

In this study, an attempt to investigate the influence of penetration angles (PAs), 5:5:90°, on the GTHP of STHEs with MSTG configurations, utilizing CDTG and DCTG configurations under different mass flow rates was made. The numerical simulations were conducted with ANSYS Fluent 19.2 software. The results of the simulation in terms of global thermo-hydraulic performance indices, for the heat exchangers geometry were determined. Comparing STHE-MSTG to conventional STHE-STG, the numerical results showed a significant improvement in the thermo-hydraulic performance of STHEs with a significant increase in GTHP. This is due to a notable drop in the recirculation flow magnitude when compared to a typical STHE with STG integrated with segmental baffles. Concerning the comprehensive performance, the multi-cross-sectional shell-and-tube heat exchangers with a 5° angle of penetration far outweigh that of the other heat exchangers investigated. The thermo-hydraulic performance indices of STHE with CTDG were 50 - 53%, 30 - 40%, 48 - 48.5%, 62 - 62.5%, 45 - 45.4%, 58 - 58.3 % and 76 - 76.8% better than the baseline (STHE-STG) in terms of WSGPF, WPEI, WTPF, WPEC, WSHTC, WFSN and  $\epsilon$ , respectively, under the same mass flow rate. Thus, the multi-cross-sectional shell-and-tube heat exchangers can be used as an alternative to the baseline to have a reliable, improved, efficient, and cost-effective processing plant.

#### REFERENCES

- Ajaykumar, V., Titus, R. and Sudhakar, T. (2016). Computational and experimental investigation of shell and tube heat exchanger with finned tubes under various flow rates. *International Journal for Innovative Research in Science & Technology*, 3(01), 191-196.
- Alabi, I. O., Dare, A. A. and Petinrin, M. O. (2024). Influence of multi-cross sectional tube configurations on thermo-hydraulic performance of shell and tube heat exchangers. *Book of Proceedings, 2nd Faculty of Engineering and Technology Conference (FETiCON 2024)*, June. 2 - 6, 2024, University of Ilorin, Nigeria, 595-605.
- Alfarawi, S. (2020). Evaluation of hydro-thermal shell-side performance in a shell-and-tube heat exchanger: cfd approach. *Journal of Advanced Research in Fluid Mechanics and Thermal Sciences*, 66(1), 104-119
- Bergman, T. L., Lavine, A. S., Incropera, F. P. and Dewitt, D. P. (2011). *Fundamentals of heat and mass transfer* (7th ed.). John Wiley and Sons.
- Du, T. and Du, W. (2019). Characteristics of flow and heat transfer of shell-and-tube heat exchangers with overlapped helical baffles. *Front. Eng. Manag.*, 6(1), 70–77. <https://doi.org/10.1007/s42524-019-0005-8>.
- Gondane, R. and Jibhakate, Y. M. (2018). Design and CFD analysis of shell and tube heat exchanger using plain tube and corrugated tube. *IJARIE*, 4(3), 2192- 2199.
- Harish, R., Santosh, G., Rudragouda, R P. and Santoshkumar, V. (2018). Design, manufacturing, and testing of shell and tube heat exchanger and to compare the performance using plain tubes and lowfin tubes. *International Journal of Research in Engineering and Technology*, 7(9), 47-51. <https://doi.org/10.15623/ijret.2018.0709006>

- Jiao, F., Wang, M., Hu, M. and He, Y. (2022). Structural optimization of self-supporting rectangular converging-diverging tube heat exchanger. *Energies*, 15, 1133. <https://doi.org/10.3390/en15031133>.
- Kececy, F. J. (2008). Coupling momentum and continuity increases CFD robustness. *ANSYS Advantage*, 2(2), 49-51.
- Kuppan, T. (2013) *Heat exchanger design handbook* (2nd ed.). Taylor and Francis.
- Li, N., Chen, J., Cheng, T., Klemes, J. J., Varbanov, P. S., Wang, Q., Yang, W., Liu, X., and Zeng, M. (2020). Analysing thermal-hydraulic performance and energy efficiency of shell-and-tube heat exchangers with longitudinal flow based on experiment and numerical simulation, *Energy*, 202, 117757. <https://doi.org/10.1016/j.energy.2020.117757>
- Luo, X., Chen, B., Min, M., Jin, M., and Liu, H (2021). Numerical simulation of shell and tube heat exchanger based on fluent. *IOP Conf. Series: Earth and Environmental Science*, 791, 1-5. <https://doi.org/10.1088/1755-1315/791/1/012084>
- Mohammad, M.H., Abbasi, H.R., Yavarinasab, A. and Pourrahmani, H. (2020). Thermal optimization of shell and tube heat exchanger using porous baffles. *Applied Thermal Engineering*, 170, 2-17. <https://doi.org/10.1016/j.applthermaleng.2020.115005>
- Mukherjee, R. (1998). Effectively Design Shell-and-Tube Heat Exchangers. *Chemical Engineering Progress*.(February).
- Naqvi, S.M.A. and Wang, Q. (2019). Numerical comparison of thermohydraulic performance and fluid-induced vibrations for sthxs with segmental, helical, and novel clamping antivibration baffles. *Energies*, 12(540), 1-18. <https://doi.org/10.3390/en12030540>
- Olaiya, K. A., Alabi, I. O., Okediji, A. P. and Alonge O. I. (2018). Parametric and quantitative analysis on the development of shell and tube heat exchanger. *International Journal of Advanced Engineering, Management and Science*, 4(6), 451-459. <https://dx.doi.org/10.22161/ijaems.4.6.4>
- Petinrin, M. O. and Dare, A. A. (2020). Numerical and experimental investigation on performance of convex-cut baffles in shell-and-tube heat exchanger. *Journal of Engineering Research and Reports*, 13(3), 8-26. <https://doi.org/10.9734/JERR/2020/v13i31710>  
1. Retrieved May 30, 2023.
- Petinrin, M.O. (2016). Performance characteristics of shell-and-tube heat exchangers with selected baffle configurations (PhD thesis). *Department of Mechanical Engineering, University of Ibadan, Nigeria*.
- Prabakaran, S., Manojprabhakaran, G. and Gopi, P. (2016). CFD integrated optimum design and prototyping of shell and tube heat exchanger. *Global Research and Development Journal for Engineering*, 1(4), 38-48.
- Saffarian, M. R., Fazelpour, F. and Sham, M. (2019). Numerical study of shell and tube heat exchanger with different cross-section tubes and combined tubes. *International Journal of Energy and Environmental Engineering*, 1-14. <https://doi.org/10.1007/s40095-019-0297-9>
- Shahril, S.M., Quadir, G.A., Amin, N.A.M. and Badruddin, I.A. (2017). Thermo hydraulic performance analysis of a shell-and-double concentric tube heat exchanger using CFD. *International Journal of Heat and Mass Transfer*, 105, 781-798. <http://dx.doi.org/10.1016/j.ijheatmasstransfer.2016.10.021>
- Shirvan, K. M., Mamourian, M. and Esfahani, J. A. (2018). Experimental investigation on thermal performance and economic analysis of cosine

wave tube structure in a shell and tube heat exchanger. *Energy Conversion and Management*, 175, 86–98.

<https://doi.org/10.1016/j.enconman.2018.08.103>

Sinnott, R. K. (2005). *Chemical Engineering Design* (4th ed., Vol. 6). Butterworth-Heinemann.

Slimene, M. B., Poncet, S., Bessrou, J., and Kallel F. (2021). Numerical modelling of a rectangular shell-and-tube heat exchanger, *Proceedings of the 6th World Congress on Momentum, Heat and Mass Transfer (MHMT'21) Lisbon, Portugal Virtual Conference*, June 17 – 19, 2021, Paper No. ENFHT 306, 1-8.

<https://doi.org/10.11159/enfht21.lx.306>

Slimene, M.B., Poncet, S., Bessrou, J. and Kallel F. (2022). Numerical investigation of the flow dynamics and heat transfer in a rectangular shell-and-tube heat exchanger. *Case Studies in Thermal Engineering*, 32, 101873.

<https://doi.org/10.1016/j.csite.2022.101873>.

Wang, G., Wang, D., Peng, X., Han, L., Xiang, S. and Ma, F. (2018). Experimental and numerical study on heat transfer and flow characteristics in the shell side of helically coiled trilobal tube heat exchanger. *Applied Thermal Engineering*.

<https://doi.org/10.1016/j.applthermaleng.2018.11.055>

Zahid, H. B., Mubashar, A., Waqas, M., Siddiqi, M. H., Munir, U. and Abbas, N. S. M. (2023) Experimental and CFD simulation study of shell and tube heat exchangers with different baffle segment configurations. *Thermal Science*, 27(1B), 843-853.

<https://doi.org/10.2298/TSCI220124075Z>

Retrieved on 25/6/2023.

APPENDIX A

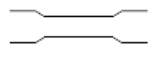
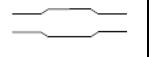
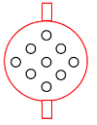


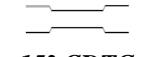



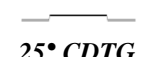

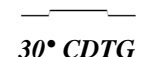







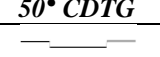

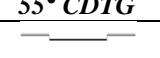
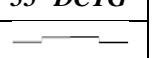
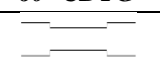

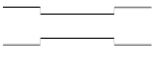

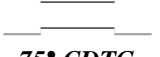
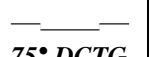




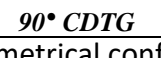
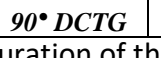


<b>STG (baseline)</b>			 <b>30° Tube layout</b>
	<b>5° CDTG</b>	<b>5° DCTG</b>	
			
	<b>10° CDTG</b>	<b>10° DCTG</b>	
			
	<b>15° CDTG</b>	<b>15° DCTG</b>	
			
	<b>20° CDTG</b>	<b>20° DCTG</b>	
			
	<b>25° CDTG</b>	<b>25° DCTG</b>	
			
	<b>30° CDTG</b>	<b>30° DCTG</b>	
			
	<b>35° CDTG</b>	<b>35° DCTG</b>	
			
<b>40° CDTG</b>	<b>40° DCTG</b>		
			
<b>45° CDTG</b>	<b>45° DCTG</b>		
			
<b>50° CDTG</b>	<b>50° DCTG</b>		
			
<b>55° CDTG</b>	<b>55° DCTG</b>		
			
<b>60° CDTG</b>	<b>60° DCTG</b>		
			
<b>65° CDTG</b>	<b>65° DCTG</b>		
			
<b>70° CDTG</b>	<b>70° DCTG</b>		
			
<b>75° CDTG</b>	<b>75° DCTG</b>		
			
<b>80° CDTG</b>	<b>80° DCTG</b>		
			
<b>85° CDTG</b>	<b>85° DCTG</b>		
			
<b>90° CDTG</b>	<b>90° DCTG</b>		

Figure A. Geometrical configuration of the tubes

APPENDIX B

Table A: Performance Criteria

Performance criteria	Weighted form
$\text{TPF} = \frac{\text{Nu}_{\text{new}}/\text{Nu}_{\text{control}}}{\left(\frac{f_{\text{new}}}{f_{\text{control}}}\right)^{1/3}}$	$\text{WTPF} = \frac{\text{TPF}_{\text{new}} - \text{TPF}_{\text{control}}}{(\text{TPF}_{\text{new}} + \text{TPF}_{\text{control}})/2}$
$\text{SGPF}, \Gamma = \frac{\left(\frac{h}{\Delta P}\right)_{\text{new}}}{\left(\frac{h}{\Delta P}\right)_{\text{straighttube}}}$	$\text{WSGPF} = \frac{\text{SGPF}_{\text{new}} - \text{SGPF}_{\text{control}}}{(\text{SGPF}_{\text{new}} + \text{SGPF}_{\text{control}})/2}$
$\text{PEI}, \eta = \frac{h}{\Delta P^{1/3}}$	$\text{WPEI} = \frac{\text{PEI}_{\text{new}} - \text{PEI}_{\text{control}}}{(\text{PEI}_{\text{new}} + \text{PEI}_{\text{control}})/2}$
$\text{PEC} = \frac{\dot{Q}_{\text{new}}/\dot{Q}_{\text{control}}}{\left(\frac{\Delta P_{\text{new}}}{\Delta P_{\text{control}}}\right)^1}$	$\text{WPEC} = \frac{\text{PEC}_{\text{new}} - \text{PEC}_{\text{control}}}{(\text{PEC}_{\text{new}} + \text{PEC}_{\text{control}})/2}$
$F_{\text{SN}} = \frac{\text{Nu}_s}{\text{Re}_s \text{Pr}_s}$	$\text{WFSN} = \frac{\text{WFSN}_{\text{new}} - \text{WFSN}_{\text{control}}}{(\text{WFSN}_{\text{new}} + \text{WFSN}_{\text{control}})/2}$
$\text{WSHTC} = \frac{h_{\text{new}} - h_{\text{control}}}{(h_{\text{new}} + h_{\text{control}})/2}$	
$\varepsilon = \frac{\dot{Q}}{\dot{Q}_{\text{max}}} = \frac{T_{h,\text{in}} - T_{h,\text{out}}}{T_{h,\text{in}} - T_{c,\text{in}}}$	

APPENDIX C

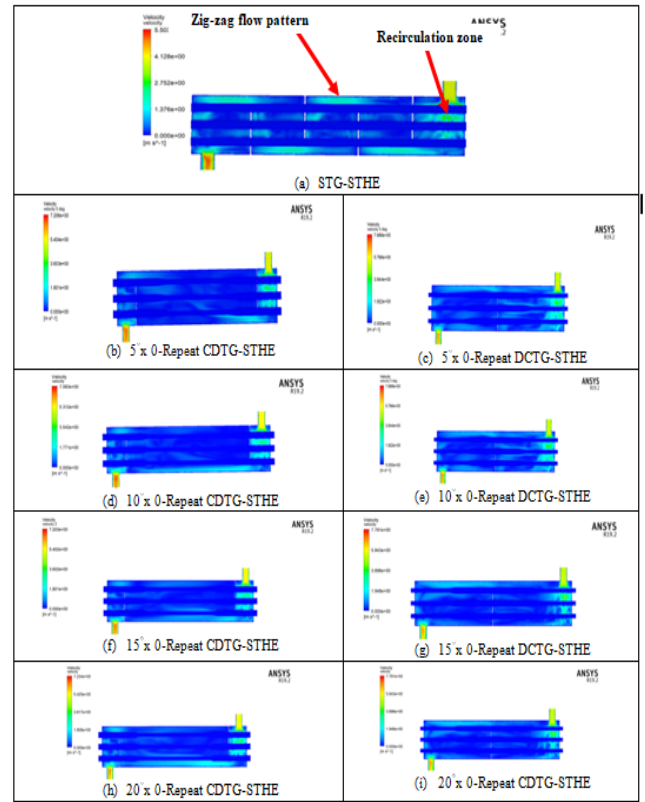


Figure B. Velocity map for STHE-MSTG at different Penetrating Angles (PAs)